

WEAK GRAVITATIONAL LENSING BY A SAMPLE OF
X-RAY LUMINOUS CLUSTERS OF GALAXIES – III.
SERENDIPITOUS WEAK LENSING DETECTIONS OF DARK AND LUMINOUS MASS
CONCENTRATIONS.

HÅKON DAHLE^{1,2,3}

NORDITA, Blegdamsvej 17, DK-2100, Copenhagen Ø, Denmark

KRISTIAN PEDERSEN

Astronomical Observatory, University of Copenhagen
Juliane Maries Vej 30, DK-2100, Copenhagen Ø, Denmark

PER B. LILJE

Institute of Theoretical Astrophysics, University of Oslo
P.O. Box 1029, Blindern, N-0315 Oslo, Norway

STEVE J. MADDIX

School of Physics and Astronomy, University of Nottingham
University Park, Nottingham, NG7 2RD, UK

AND

NICK KAISER

Institute for Astronomy, University of Hawaii
2680 Woodlawn Drive, Honolulu, Hawaii 96822

ApJ, in press

ABSTRACT

In the course of a weak gravitational lensing survey of 39 clusters of galaxies, covering a total sky area of ~ 1 square degree, we have serendipitously discovered mass concentrations in the fields of A1705 and A1722 which are most probably not associated with the main cluster target. By combining weak lensing information with two-color galaxy photometry in fields centered on our sample clusters, we identify a new cluster candidate at $z \sim 0.5$ in the field of A1705. This cluster candidate also displays strong lensing in the form of a giant luminous arc. The new mass concentration in the field of A1722 also seems to be associated with an optically luminous cluster of galaxies at $z \sim 0.5$, but in this case there is some evidence for additional structures along the line of sight that may contribute to the lensing signal. A third cluster, A959, has a dark sub-clump which shows interesting morphological evidence in the mass map for being associated with the main cluster. This is the first case where there is any significant evidence for a physical association between a dark sub-clump (discovered from weak lensing) and a normal cluster. Analysis of archival X-ray data shows that the three new mass concentrations are not firmly detected in X-rays and that they are X-ray underluminous.

Subject headings: Cosmology: observations — dark matter — gravitational lensing — Galaxies: clusters

1. INTRODUCTION

Weak gravitational lensing provides a powerful way to identify cluster-sized density peaks in the Universe, independent of their baryonic content. Given the currently modest sky coverage of optical imaging surveys with the depth and image quality required to detect new clusters by their weak lensing effect, the number of currently known mass-selected clusters is very small. It is still an open question whether the mass-selection will lead to the identification of a population of clusters which are physically different from optically selected clusters or X-ray detected clusters. If a population of “baryon-poor” clusters is found to exist, they may be very useful laboratories for the study of dark matter properties. For instance, some dark matter candidates such as sterile neutrinos may produce an observable signature from their decay (Abazajian, Fuller, & Tucker 2001). The best

places to detect such a signature would be in baryon-poor clusters – if such objects exist – where the spectral line corresponding to dark matter decay would be relatively more conspicuous compared to the emission produced by bremsstrahlung in the hot intra-cluster gas (Hansen et al. 2002). In any case, the existence of baryon-poor clusters or sub-clusters would pose a challenge to current models for structure formation. Furthermore, any previously unrecognized population of clusters with high mass-to-light ratios would have to be taken into account when using the measured average mass-to-light ratios of clusters to estimate the density parameter Ω_m .

The present sample of weak lensing-detected clusters is small and contains both clusters with “normal” mass-to-light ratios and objects which appear to be optically dark. From weak lensing observations in the field of the cluster A1942, Erben et al. (2000) find a secondary mass peak $\sim 7'$ south of the cluster

¹ Present address: Institute of Theoretical Astrophysics, University of Oslo, P.O. Box 1029, Blindern, N-0315 Oslo, Norway; hdahle@astro.uio.no

² Also at: Institute for Astronomy, University of Hawaii

³ Visiting observer, University of Hawaii 2.24m Telescope at Mauna Kea Observatory, Institute for Astronomy, University of Hawaii

center which does not correspond to any strong concentration of bright galaxies. From deep H -band imaging of this region, Gray et al. (2001) constrain the bolometric mass-to-light ratio to be $M/L_{\text{Bol}} > 1000h$ in solar units for any reasonable lens redshift. Umetsu & Futamase (2000) find a dark mass concentration 1.7 south of the high-redshift cluster CL1604+4304 ($z = 0.90$) with an estimated mass of $1.2 \times 10^{14} h^{-1} M_{\odot}$ and $M/L_B \geq 1000h$ in solar units, if it is located at the redshift of CL1604+4304. At present, it is not clear whether the dark clumps found by Erben et al. and Umetsu & Futamase are physically associated with the nearby clusters, or whether they represent chance alignments on the sky of objects at different redshifts. Most recently, Miralles et al. (2002) have reported evidence for another dark cluster from a conspicuous alignment of faint galaxies in a parallel STIS pointing adjacent to the local Seyfert galaxy NGC 625.

Wittman et al. (2001) report the discovery of a more “normal” cluster in a “blank sky” field through a combination of weak gravitational lensing and photometric data. Their $BVRI$ photometry shows a concentration of elliptical galaxies close to the lensing-derived mass peak corresponding to the cluster, and spectroscopic follow-up of candidate cluster members reveals a cluster with modest galaxy velocity dispersion ($\sigma_v = 615 \pm 150 \text{ km s}^{-1}$) at $z = 0.28$. The mass-to-light ratio of this cluster is $M/L_R = 560 \pm 200h$, which is somewhat high compared to average values of $M/L_B \approx 300h$ obtained from both virial and weak lensing analyses of X-ray selected clusters (e.g., Carlberg et al. 1997; Hoekstra et al. 2002; Dahle et al. 2003, in prep.), but there are some X-ray selected clusters with similar lensing-derived M/L , such as MS 1224.7+2007 at $M/L_R = 640 \pm 150$ (Fahlman et al. 1994; Fischer 1999), and A68 and A697 at $M/L_R = 680 \pm 230h$ and $M/L_R = 450 \pm 115h$, respectively (Dahle et al. 2003, in prep.).

In Paper I in this series (Dahle et al. 2002) we presented weak lensing measurements of a sample of 39 X-ray selected clusters. The results were presented in the form of maps of the reconstructed projected matter density ($\kappa = \Sigma/\Sigma_{\text{crit}}$, where Σ_{crit} is the critical surface mass density for lensing) and in the form of radial mass profiles around each (lensing-determined) cluster center. Several mass maps show evidence for sub-peaks in the mass distribution which are not associated with obvious sub-clumping of optically luminous galaxies inside the cluster. In this paper, we investigate the properties of the most significant of these sub-peaks. We attempt to constrain the redshift and mass-to-light ratio of these systems and discuss whether they are likely to be physically associated with their apparent “host clusters”.

In §2 we describe the selection criteria for cluster candidates, which we describe individually in §3. In §4 we compare our new (sub-)cluster candidates to those found by other groups, and compare the observed abundances and physical properties of such objects to recent theoretical predictions.

The numbers in this paper are given for an Einstein-de Sitter ($\Omega_m = 1, \Omega_{\Lambda} = 0$) cosmology. The Hubble parameter is given by $H_0 = 100h \text{ km s}^{-1} \text{ Mpc}^{-1}$, and all celestial coordinates are given in J2000.0.

2. IDENTIFICATION OF NEW CLUSTER CANDIDATES

In Paper I we described a data set of weak lensing measurements of 39 clusters in the redshift range $0.15 < z < 0.35$, with selection based on very high X-ray luminosity ($L_{x,0.1-2.4\text{keV}} \geq 10^{45} \text{ erg s}^{-1}$). Most of the sky coverage of this survey comes

from imaging of fourteen clusters with the UH8K mosaic CCD camera at the 2.24m University of Hawaii Telescope at Mauna Kea Observatory, which gives a $19'$ field when mounted at the $f/10$ Cassegrain focus (see Paper I for a complete list of the observations). The imaging data were reduced according to the “pipeline” reduction procedure for mosaic CCD data described by Kaiser et al. (1999), and the weak gravitational lensing was measured using the shear estimator introduced by Kaiser (2000). The reduction and analysis procedures used are described in detail in Paper I.

In some of the reconstructed mass maps of the fields observed with the UH8K camera, there are secondary mass peaks which appear significant when compared to peaks in randomized shear maps (see Figure 48 of paper I), or peaks seen in mass reconstructions of blank fields (see Wilson, Kaiser & Lupino 2001), but do not correspond to concentrations of early-type galaxies at the cluster redshift. These may be mass concentrations corresponding to high-redshift clusters that only contribute weakly to the light distribution in the field, compared to the more nearby target clusters. At redshifts > 0.4 , the early-type galaxies at a given redshift will be significantly bluer than predicted from the approximate linear $V-I$ color-redshift relation used in Paper I. Thus, their contribution to the prediction for the dimensionless surface density given for each cluster in Paper I will be increasingly underestimated with increasing redshift.

An even more interesting possibility is that these are optically and/or X-ray dark clusters at intermediate redshifts (or dark sub-clumps physically associated with their apparent host clusters), i.e., mass concentrations that have much higher M/L values than normal clusters.

2.1. Lensing Cluster Search

As noted in Paper I, the 1σ level of noise in the random mass maps is in the range $0.035 < \kappa < 0.05$, mostly depending on seeing. Given the large number of fields covered by our survey, we may expect to see maybe one or two 3σ peaks that are generated by random noise due to the intrinsic galaxy shapes. However, the reality of a mass peak at this level will become significantly more certain if it can be shown to be strongly correlated with clustering in the visible galaxy distribution, or with a peak in the X-ray luminous gas.

From the reconstructions of the dimensionless projected mass surface density κ presented in Paper I, we select candidates for additional mass concentrations using the following criteria:

- The dimensionless projected surface density κ should be > 0.15 (corresponding to a $> 3\sigma$ detection of mass even in the fields with the highest noise) at the position of the peak. This selection criterion was applied to mass maps derived separately from V - and I -band imaging data, and to mass maps derived from a combination of the two, as detailed in Paper I. We found a total of three mass peaks which are above the κ threshold in at least one of the different mass maps and which also satisfy the other three selection criteria below.
- The mass peak should be clearly separated (with offset $> 1'$) from the mass peak that corresponds to the light peak/optical cluster center (or any other significant peak in the light distribution of galaxies belonging to

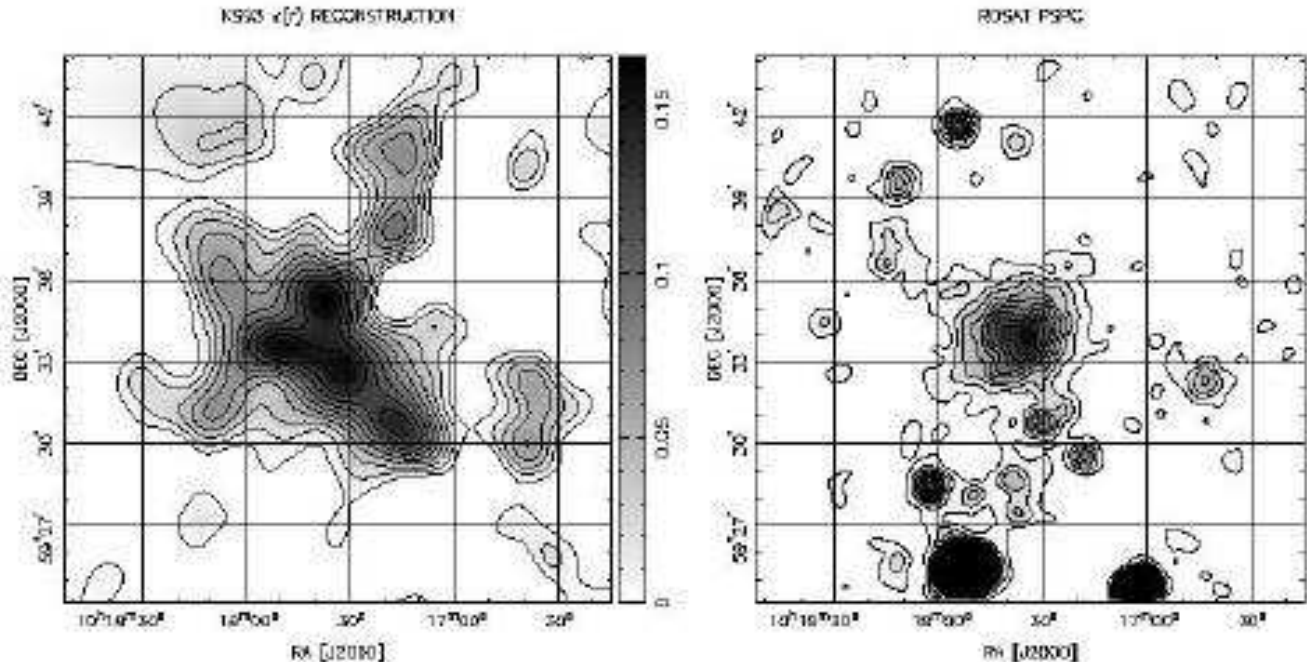


FIG. 1.— Left panel: The reconstructed projected mass density in the field of A959. The mass map is based on the KS93 inversion method, with a Gaussian smoothing scale of $47''$. The scale bar on the right runs from zero to the peak value of κ . The plotted contours start at zero and are spaced at intervals of $\Delta\kappa = 0.017$. Right panel: A 15.4 ksec ROSAT PSPC exposure in the 0.1 – 2.4 keV energy band, smoothed with a Gaussian of scale $13''/5$ (9 pixels). The 10 contour levels are plotted on a linear scale ranging from 1.2×10^{-4} counts/sec to 9×10^{-4} counts/sec.

a previously known cluster, as determined from their $V-I$ colors).

- Both V - and I -band photometry should be available at the position of the clump. Given the data set of Paper I, this implies that the total sky coverage of our search is 1.0 deg^2 . The dominant contribution to the sky coverage comes from $\sim 19'$ wide UH8K fields, and all the mass peaks discussed here are located in such fields.
- Candidates within $1'$ from the field edges are discarded, as the noise in weak lensing reconstructions are known to increase close to the edges.

The limit on the value of the mass surface density κ is partly motivated by the study of Wilson, Kaiser & Luppino (2001), who present weak lensing data of similar quality to the data set used in this paper for 1.5 deg^2 of “blank sky”. See Kaiser, Wilson & Luppino (2000) and Paper I for more details about the characteristics of each data set. After smoothing their reconstructed mass maps with a $45''$ Gaussian filter (we use a $47''$ Gaussian filter) they do not find any pixel values above $\kappa = 0.15$. If the sky density of optically dark high-density mass peaks was found to be significantly higher in the fields of known clusters (e.g., the fields studied in Paper I) than in blank fields (e.g, the fields of Wilson et al. 2001), it would be a clear indication of a physical association between the dark clumps and “normal” clusters.

We note that the mass maps presented in this paper differ slightly from the mass maps presented for the same clusters in Paper I. The difference is in the relative weighting of shape measurements of faint galaxies in the two passbands when estimating the shear. In Paper I, the mass reconstruction was based

on shear estimates from a combined “ $V+I$ ” catalog which was made by selecting the catalog entry from the passband in which the object was detected with the highest significance. The maps presented in this paper are generated by taking a weighted average (where the weights are given by the “figure of merit” values $\sum Q^2/d\Omega$; see Paper I and Kaiser 2000) of this “ $V+I$ ” mass map and the mass maps generated separately from the I -band and V -band catalogs. The 1σ level of noise in these maps at the positions of the newly discovered mass peaks is $\kappa = 0.03$.

2.2. Photometric cluster search

For the UH8K fields which have both I -band and V -band data covering the whole field, the nature of the lensing-derived mass peaks can be investigated by looking for associated concentrations of red galaxies, corresponding to galaxy clusters up to $z \sim 1$.

Our photometric procedures are described in Paper I and are only briefly recounted here. We used SExtractor (Bertin & Arnouts 1996) to derive total V - and I -band magnitudes for galaxies in the fields, and we also measured a $V-I$ color within a fixed aperture of $2''/7$. The reason for calculating the color within this smaller aperture rather than based on the total magnitudes is that the aperture magnitudes are less sensitive to contamination by other objects and to color gradients within the galaxies themselves and thus yield a tighter red sequence in a color-magnitude diagram. The magnitudes were corrected for Galactic extinction using the dust maps of Schlegel, Finkbeiner & Davis (1998), assuming an $R_V = 3.1$ extinction curve.

To identify optical cluster candidates based on our two-filter photometry, we used a simplified version of the cluster-red-sequence (CRS) method used by Gladders & Yee (2000) for their Red-Sequence Cluster Survey. This cluster finding algo-

rithm takes advantage of the fact that early-type galaxies in dense cluster environments form a remarkably tight, almost horizontal sequence in their color-magnitude diagrams, and these sequences are strongly homogeneous at a given redshift (e.g., Smail et al. 1998; Gladders & Yee 2000 and references therein). Also, at redshifts $z \lesssim 1$ the early-type galaxies that form the red cluster sequence will have a redder $V-I$ color than any other normal galaxies at redshifts equal to, or lower than, the redshift of the cluster.

The basic idea behind the CRS method is to create a series of smoothed maps of the galaxy density in the field by selecting galaxies in a series of partially overlapping slices in the color-magnitude diagram. Gladders & Yee (2000) used color slices defined by theoretical predictions of the red sequence, but we choose here to neglect the slope of the red sequence and use a series of horizontal slices evenly spaced in $V-I$. Both theoretical predictions from population synthesis models and empirical results based on our data set show the absolute value of the red-sequence slope to be less than 0.1 per I -magnitude. Given the relatively narrow magnitude range (particularly at high redshifts) of cluster galaxies contributing to a given slice, and the fact that our color slices are approximately twice as wide as those used by Gladders & Yee (2000), the effect of the slope will not significantly influence our ability to detect cluster candidates with this algorithm. However, it would probably bias redshift estimates of cluster candidates, but only at levels comparable to the systematic uncertainty introduced by the photometric calibration of the UH8K mosaic camera (we note that the photometric stability of the CCD chips in the UH8K is questionable at the $\lesssim 0.1$ magnitude level).

For each slice, we include all galaxies at $I < 23$ that have a probability higher than 10% of really belonging to that slice when taking the photometric uncertainties into account. The width of the slices was $\Delta(V-I) = 0.3$ at bright magnitudes and slightly larger at faint magnitudes due to the increasing photometric uncertainties. This is about twice the measured intrinsic width of the red sequence (Stanford, Eisenhardt, & Dickinson 1998).

Rather than using a more elaborate galaxy weighting scheme such as the one outlined by Gladders & Yee (2000), we chose a simple faint galaxy cutoff at $I = 23$. Also, to generate smoothed galaxy number density plots comparable to the weak lensing-derived mass maps, we employed a Gaussian smoothing kernel of fixed scale $47''$ rather than a kernel tailored to fit the expected cluster density profile at a given redshift. The primary purpose of generating these plots is to search for galaxy density enhancements at the position of the lensing-detected cluster candidates.

2.3. Lensing masses and mass-to-light ratios

For each (sub-)cluster candidate, the (minimum) mass and the mass-to-light ratio were estimated within an aperture centered on the corresponding peak found in the κ map (see Table 1). A lower limit on the aperture mass was found using the aperture densitometry statistic ζ of Kaiser et al. (1994):

$$\zeta(R_1, R_2) = \bar{\kappa}(R_1) - \bar{\kappa}(R_1, R_2) = \frac{2}{1 - R_1^2/R_2^2} \int_{R_1}^{R_2} \langle \gamma_T \rangle d \ln r, \quad (1)$$

which measures the average surface mass density within an aperture radius $R_{\text{ap}} = R_1$ minus the average surface mass density in a surrounding annulus $R_1 < R < R_2$ (here, γ_T is the tangential component of the shear). Hence, a lower limit on the

aperture mass can be simply calculated as $M_{\text{ap}} = \pi r^2 \zeta \Sigma_{\text{crit}}$. We chose $R_2 = 2R_1$, and our estimate of M_{ap} will in this case e.g., underestimate the true aperture mass by 33% for an isothermal sphere ($\Sigma \propto R^{-1}$) mass distribution.

In order to minimize the bias caused by the presence of a more massive cluster in each field we chose to use an outer radius R_2 much smaller than the R_2 values used for the aperture mass measurements presented in Paper I. For this reason, R_2 was chosen to be less than half the angular separation between the new cluster candidate and the Abell cluster. For this geometry, we find from simple simulations that the aperture mass measurement is affected by $< 1\%$, provided that the mass of the Abell cluster is not more than twice that of the new cluster candidate. In the case of the A959 and A1705 fields, we used a control annulus with $R_2 = 2'$ and inner radius $R_1 = 1'$. The cluster candidate in the A1722 field had a somewhat larger separation from its host cluster, and it was therefore possible to use a larger aperture with $R_2 = 4'$ and $R_1 = 2'$. By defining an aperture measurement of the surface light density ζ_L in a manner similar to equation (1) (i.e., generating an aperture luminosity estimate by subtracting the average galaxy luminosity density in the annulus $R_1 < R < R_2$ from the average galaxy luminosity density at $R < R_1$), the mass-to-light ratio of the mass peak can be estimated. Thus, in contrast to M_{ap} , this ratio will not be systematically underestimated.

2.4. Hot gas content

In X-ray luminous clusters of galaxies, such as those in the cluster sample of Paper I, most of the baryonic mass is in the form of hot, X-ray emitting gas (e.g., Ettori & Fabian 1999). In order to constrain the hot gas content of the (sub-)cluster candidates we analyzed the best quality archive X-ray data (standard screened EINSTEIN IPC, ROSAT PSPC and ASCA SIS data, respectively) for these candidates. No obvious X-ray emission is associated with any of the (sub-)cluster candidates so we determine upper limits for their X-ray luminosity as described below.

An upper limit for the (sub-)cluster X-ray count rate is extracted within two apertures: The aperture as determined from the weak lensing maps (R_{ap}) and the radius within which the average (sub-)cluster mass density is 500 times the critical density of the Universe (r_{500}). Special care is taken in estimating the background.

For EINSTEIN IPC data (A1705) and ROSAT PSPC data (A959) the background is estimated from the data set including the new mass concentration itself. The background is calculated as the average of three source-free regions of the same size as the (sub-)cluster region, and at the same optical axis distance.

For ASCA SIS data (A1722) the background count rate is evaluated from the publically available ‘‘blank sky’’ data in a two stage process: A first background estimate is obtained using exactly the same region on the SIS chip as the (sub-)cluster region. Then, the general background level in the ‘‘blank sky’’ data is compared to the general background level in the (sub-)cluster data by calculating the average count rate within three regions of the same size as the region of interest, at the same optical axis distance and devoid of obvious X-ray sources. The initial background estimate is then corrected for the average difference in background level between the ‘‘blank sky’’ data and the (sub-)cluster data. Finally, data from the SIS0 detector and the SIS1 detector are merged into one common SIS data set.

For each (sub-)cluster, we derive net count rates (corrected

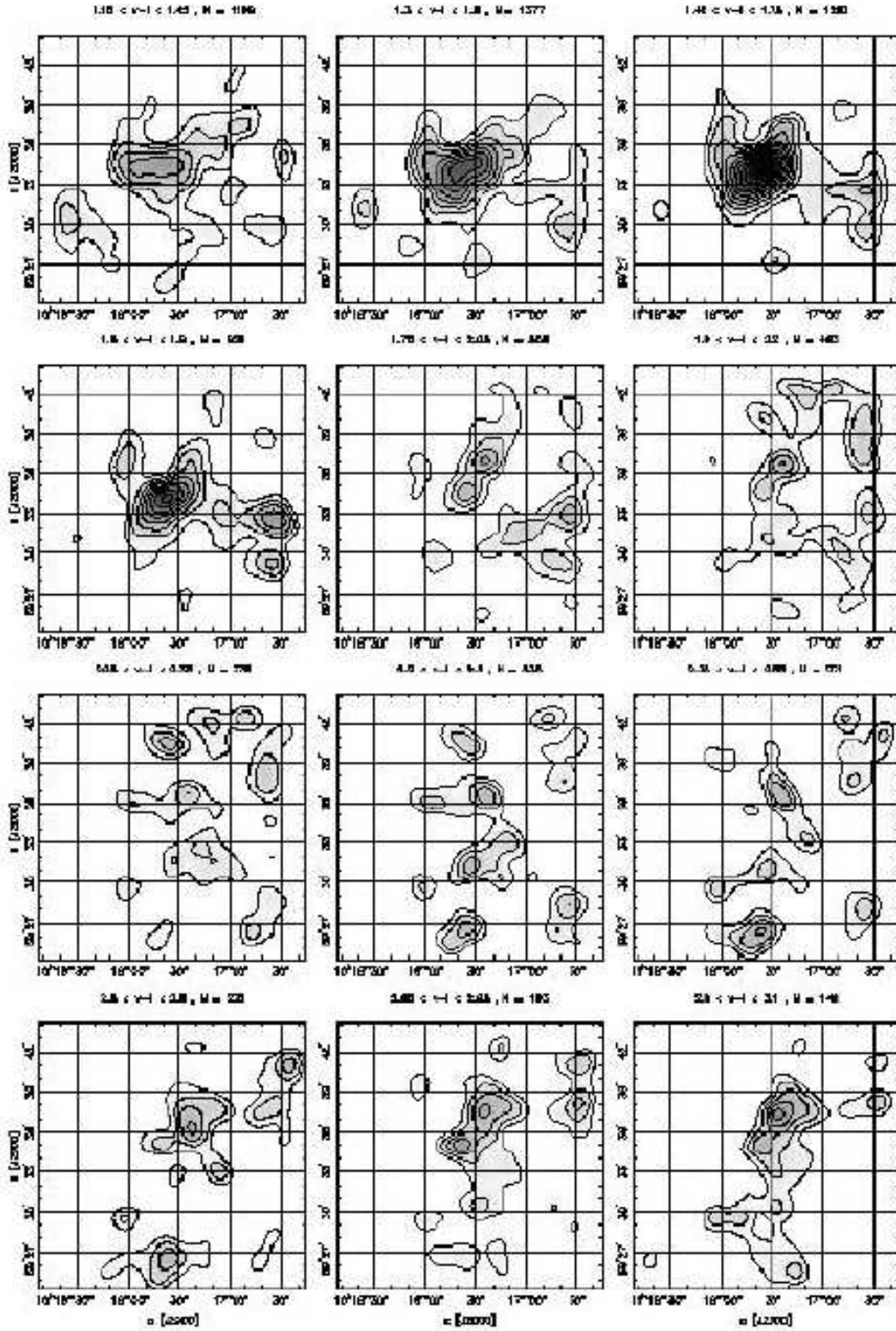


FIG. 2.— The surface number density distribution of $I < 23.0$ galaxies in various $V-I$ color intervals in the field of A959. Shown above each plot is the color interval and the number of galaxies in that interval. The plots have been smoothed with a Gaussian of scale $47''$ to yield a resolution similar to the mass map. The average level has been set to zero, and the contour levels are plotted at $1, 2, 3, \dots$ times the rms fluctuation in field galaxy density in the given color interval. The lack of galaxies in the upper left (northeastern) part of the field is an effect of the missing data from chip 4 in the UH8K mosaic.

for point source contributions) within the two apertures and convert these to 0.1 – 2.4 keV fluxes using PIMMS and an absorbed Raymond-Smith spectral model with the following parameters: Abundance is $Z = 0.25Z_{\odot}$, absorption by neutral hydrogen is fixed at the Galactic value (from Dickey and Lockman 1990), and for each (sub-)cluster the temperature is fixed at the value derived from the weak lensing mass within r_{500} using the mass-temperature relation of Finoguenov et al. (2001).

Assuming the redshift of the (sub-)cluster given in Table 1 based on optical data, the flux is converted to a luminosity for the desired cosmology. In order to determine the X-ray luminosity of the (sub-)clusters relative to a sample of nearby “standard” clusters, the upper limit on the 0.1 – 2.4 keV luminosity within r_{500} was compared to the expected value based on the lensing mass within r_{500} and the mass-luminosity relation of Reiprich & Böhringer (2002) (best bisector fit).

3. CANDIDATE MASS CONCENTRATIONS

The selection criteria outlined in § 2.1 produced three new cluster candidates, in the fields of A959, A1705 and A1722. To make the following discussion clearer and more concise, we introduce the naming convention “WL HHMM.M(+/-)DDMM” for these objects, where “WL” denotes a weak lensing-detected mass concentration and is followed by numbers that are based on the celestial coordinates of the objects (for epoch J2000.0), where the right ascension is given in units of hours and minutes (with one decimal) and the declination is given in units of degrees and arcminutes. For each candidate, we analyze its optical and lensing properties based on the data presented in Paper I along with X-ray data to search for emission from any associated hot gas. Table 1 summarizes the most important parameters for each cluster candidate.

3.1. The A959 Field

From spectroscopic observations at the WHT, we have determined a redshift $z = 0.286$ for this cluster (Irgens et al. 2002), significantly lower than the value usually quoted in the literature ($z = 0.353$). After properly revising its X-ray luminosity and temperature, it is found to have $L_{x,0.1-2.4\text{keV}} = 1.43 \times 10^{45}$ erg s^{-1} (Böhringer et al. 2000) and $T = 6.6$ keV (Mushotzky & Scharf 1997). A singular isothermal sphere (SIS)-model fit to the tangential shear measured out to a radius of $\sim 1.5h^{-1}$ Mpc shows that the cluster has a mass corresponding to a velocity dispersion $\sigma = 990_{-110}^{+100}$ km s^{-1} . The fit to a SIS-model is however not very good, and weak lensing mass measurements at large radii indicate that this cluster is very massive, with a projected 2D aperture mass $M_{\text{ap}}(< 1.5h^{-1}\text{Mpc}) \sim 2 \times 10^{15}M_{\odot}$ (see Paper I).

4

As noted in § 2.1, the mass maps used for the selection of mass peaks were different from those displayed in this paper. The reason for not using the new maps presented here (and lowering the selection threshold from $\kappa = 0.15$ to 0.14, which would have selected exactly the same three objects!) is that the noise is more clearly defined in the old maps. While the new maps have lower noise, this is not achieved by increasing the available sample of background galaxies, but instead by in effect taking a weighted average of the shape measurements of these galaxies in the two passbands. Hence, the photon counting noise for the shape measurements of faint galaxies is somewhat reduced, while the noise due to the finite number density of background galaxies does not change.

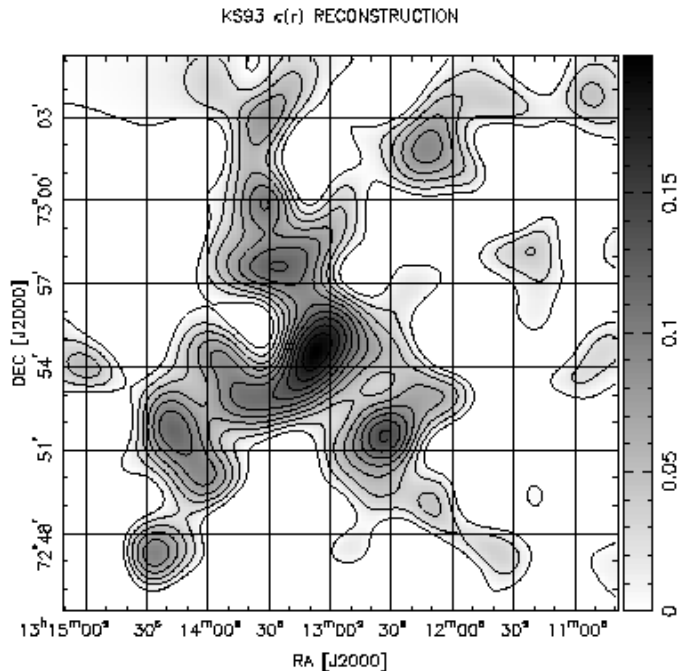


FIG. 3.— The reconstructed projected mass density in the field of A1705. The mass map is based on the KS93 inversion method, with a Gaussian smoothing scale of $47''$. The scale bar on the right runs from zero to the peak value of κ . The plotted contours start at zero and are spaced at intervals of $\Delta\kappa = 0.020$.

Optically, the cluster center is not dominated by any single galaxy, but it has a core region consisting of many early-type galaxies of similar brightnesses. A highly significant mass peak (with some evidence for substructure) is seen in the weak lensing mass map (see Figure 1), and the dark matter distribution appears to resemble the cluster light distribution, as apparent in the first four panels of Figure 2. However, there is a dark matter concentration, hereafter denoted as WL 1017.3+5931, $\sim 6'$ southwest of the cluster center which does not correspond to any peak in the luminosity distribution. Its peak value⁴ is $\kappa = 0.143$.

Due to the very low background, the ROSAT PSPC 15.4 ksec exposure yields the tightest current constraints on diffuse X-ray emission from WL 1017.3+5931. In Figure 1, a couple of X-ray sources are seen close to WL 1017.3+5931. Archival ROSAT HRI images show that sources “C” and “D” are extended sources while source “A” is a point source and source “B” consists of two point sources on top of some extended emission. This extended X-ray emission is possibly linking WL 1017.3+5931 to the main cluster of A959. The mass morphology of WL 1017.3+5931 provides clearer evidence for this link, since there appears to be a bridge of matter extending from the A959 cluster center toward WL 1017.3+5931, and the peak itself appears highly elongated in the direction toward the center of A959. Even at the lowest “saddle point” in the apparent mass bridge between A959 and WL 1017.3+5931, the projected mass density is still as high as $\kappa = 0.122$, which is 85% of the peak value at the location of WL 1017.3+5931. Simulations of the region between two cluster mass peaks with a Gaussian smoothing scale equal to that of the real mass map and with

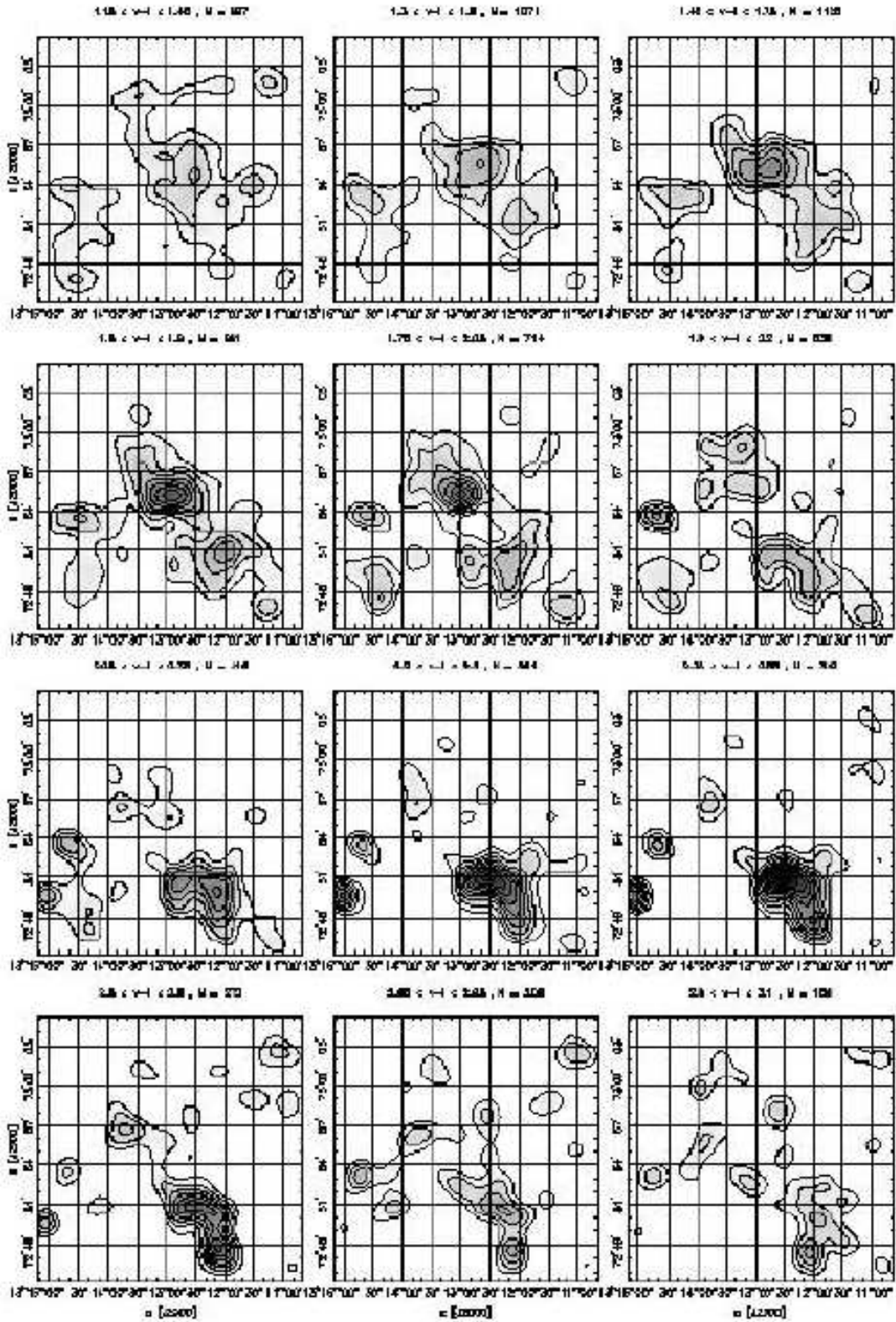


FIG. 4.— The surface number density distribution of $I < 23.0$ galaxies in various $V-I$ color intervals in the field of A1705. See the caption of Fig. 2 for details.

TABLE 1
 PROPERTIES OF THE WEAK LENSING-DETECTED MASS CONCENTRATIONS

Name	α (J2000.0)	δ (J2000.0)	Redshift z_{est}	R_{ap} (h^{-1} kpc)	M_{ap} ($10^{14}h^{-1}M_{\odot}$)	M/L_B ($h[M/L_B]_{\odot}$)	σ_{DM} ($km\ s^{-1}$)	$L_{X,ap}$ ($h^{-2}\ 10^{44}erg\ s^{-1}$)
WL 1017.3+5931	10 17 15	59 30 46	0.286?	161	1.1 ± 0.3	> 500	780^{+120}_{-160}	$< 0.008 \pm 0.006$
WL 1312.5+7252	13 12 31	72 51 32	0.55	222	2.7 ± 0.8	173 ± 54	1150^{+160}_{-190}	$< 0.09 \pm 0.03$
WL 1320.4+6959	13 20 22	69 58 43	0.45	409	4.8 ± 1.9	296 ± 118	940^{+160}_{-210}	$< 0.20 \pm 0.1$

Note. — Units of right ascension are hours, minutes and seconds, and units of declination are degrees, arcminutes, and arcseconds. The X-ray luminosity is given in the 0.1-2.4 keV band, and the uncertainty arises from poisson noise as well as point source subtraction. The values are given for an Einstein-de Sitter Universe. The source redshifts adopted for the M_{ap} estimates are based on photometric redshift data from the Hubble Deep Field (see Eq. 17 of Paper I), and correspond to having a single-screen source population at an effective redshift of $z_s = 0.7$, $z_s = 0.9$, and $z_s = 0.8$ for WL 1017.3+5931, WL 1312.5+7252, and WL 1320.4+6959, respectively

random realizations of realistic noise indicate that this feature is (marginally) significant, at almost the 2σ level. Although the reality of this feature is currently debatable, the apparent mass bridge and the ellipticity of WL 1017.3+5931 probably constitute the only significant evidence so far for a physical link between a dark sub-clump found by weak lensing in a cluster field and its apparent host cluster.

No strong galaxy overdensities are seen at the position of WL 1017.3+5931 for any of the color slices plotted in Figure 2. The lower limit value for M/L_B in Table 1 is based on an aperture light estimate using galaxies in the $2.0 < V-I < 4.0$ color range. These are all redder than the A959 cluster galaxies (the red cluster sequence has $V-I \simeq 1.7$). If we instead consider galaxies in the color range of the red cluster sequence of A959, we find that the luminosity density in the control annulus at $1' < R < 2'$ is higher than the luminosity density within $1'$, implying that there is no overdensity of light associated with A959 cluster galaxies at the location of WL 1017.3+5931. Two of the brightest galaxies in the field ($I \simeq 16.5$) are visible $2'$ from the center of WL 1017.3+5931, but these are likely to be foreground ellipticals ($V-I \simeq 1.3$), and no significant galaxy clustering is seen around these two galaxies. The estimated velocity dispersion of WL 1017.3+5931 listed in Table 1 comes from a SIS-model fit to the tangential weak shear averaged in radial bins centered on the dark clump. If WL 1017.3+5931 is at the A959 main cluster redshift, within a radius of r_{500} it is a factor three X-ray under-luminous relative to the expectation from the mass-X-ray luminosity relation of Reiprich and Böhringer (2002). However, given the scatter in the mass-luminosity relation of an order of magnitude, even though WL 1017.3+5931 is relatively X-ray dark it is still consistent with the relation. Chandra or XMM-Newton observations are required to pin down the X-ray emission of WL 1017.3+5931 and accurately constrain the hot gas content, ie. if it is really X-ray dark.

In general, there is very good morphological agreement between the mass map and hot gas as mapped by ROSAT PSPC: The mass extension towards the northeast has a clear X-ray counterpart, and at the position of the extended X-ray source “D” a mass concentration is seen. This feature also corresponds to an overdensity of galaxies (most prominent in the $1.6 < V-I < 1.9$ color slice in Figure 2) with colors similar to, or slightly redder than, the early-type galaxies in the core of A959. The general southeast-northwest elongation of the A959

cluster galaxy distribution is matched in X-rays.

We also note that there are several concentrations of red ($2.0 < V-I < 3.0$) galaxies in the field, most clearly visible in the lower three panels of Figure 2. One of these is only $\sim 1'$ north of the A959 cluster center (see the $2.65 < V-I < 2.95$ color slice in Figure 2) and may contribute to the substructure seen in the mass peak of A959.

3.2. The A1705 Field

Optical images show that the cluster center of A1705 is dominated by a single cD galaxy. The κ reconstruction of this field (see Figure 3) shows a number of secondary peaks in addition to the most significant mass peak, which is associated with the center of A1705. The position given for A1705 by Abell (1958) is $5'$ off from what we take to be the cluster center, based on the peaks in the mass, light and galaxy number density distributions, while the Zwicky cluster Zw 1312.1+7311 is more consistent with the position we determine for the A1705 cluster center (at $\alpha = 13^h13^m.0, \delta = 72^\circ55'$). The color slicing in Figure 4 shows several interesting effects: Firstly, the morphology-density relation manifests itself in the effect that the density peak associated with A1705 appears more concentrated as one moves to progressively redder color intervals (which contain the most evolved early-type cluster galaxies). This effect is also apparent in the similar plots for A959 and A1722. Secondly, the density peak of A1705 in Figure 4 shows a significant shift in the centroid position as a function of color. The galaxy number density peak is seen to move closer to the position of the mass peak for redder color intervals, and this again demonstrates that the galaxies with the most evolved stellar populations are concentrated in the densest environments. The centroid shift may indicate that A1705 is dynamically young. A secondary mass peak situated about $4'$ toward the northeast from the main peak appears to be associated with galaxies at the cluster redshift (the first five panels of Figure 4 appear to show an extension toward northeast from the main galaxy overdensity peak associated with A1705). Close to this secondary mass peak, and possibly contributing to it, is the $z = 0.112$ IRAS galaxy F13121+7315 (at $\alpha = 13^h13^m32.0^s, \delta = 72^\circ59'11''$), associated with the AGN X-ray source RX J1313.5+7259.

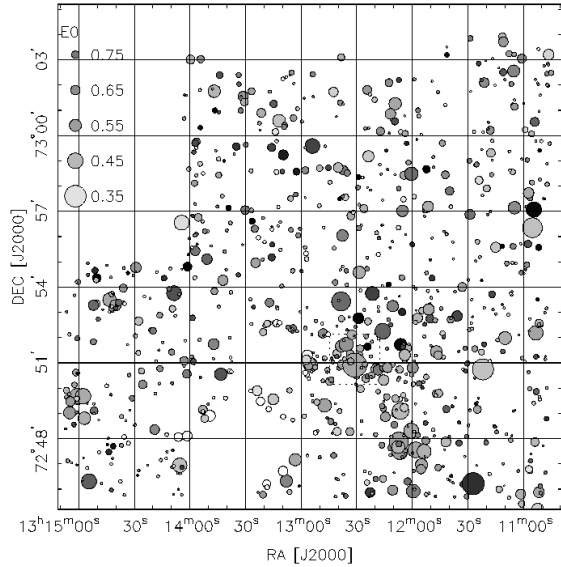


FIG. 5.— The reddest galaxies ($V-I > 2.2$) in the field of Abell 1705. The area of the circles is proportional to the I -band flux. The legend in the upper left corner indicates the flux and color (assuming no evolution of the SED) of an L_* E0 galaxy at a given redshift. The apparent lack of galaxies around $\alpha = 13^{\text{h}}13^{\text{m}}30^{\text{s}}$, $\delta = 72^{\circ}48'$ is an artifact caused by a $V = 7$ star at this position. The square region denoted by the dotted lines indicates the region shown in Fig. 6.

The two lowest rows of the galaxy number density plots in Figure 4 shows a strong peak southwest of the location of the main cluster center. This is a galaxy concentration at a redshift well beyond A1705. Figure 5 also shows this strong overdensity in the distribution of the reddest ($V-I > 2.2$) galaxies in the field. A strong concentration of galaxies with similar colors is centered on what appears to be a distant giant elliptical galaxy located at $\alpha = 13^{\text{h}}12^{\text{m}}31.1^{\text{s}}$, $\delta = 72^{\circ}50'54''$. A peak in the mass distribution, which we have named WL 1312.5+7252, is situated less than $1'$ away from this galaxy. Its peak value is $\kappa = 0.143$. A rough cluster redshift estimate can be derived for this peak from the median color ($V-I = 2.45$) of the early-type cluster galaxy sequence seen in a color-magnitude diagram. Using our empirically calibrated color-redshift relation for early-type cluster galaxies (see Figure 47 of Paper I), we estimate the redshift of the cluster associated with WL 1312.5+7252 to be $z = 0.55 \pm 0.05$. This may be a slight underestimate of the true redshift, since cluster ellipticals at $z \gtrsim 0.5$ are less evolved and intrinsically slightly bluer than their counterparts at lower redshifts (Lubin 1996).

A curved blue object, apparently a gravitationally lensed arc, is situated at $\alpha = 13^{\text{h}}12^{\text{m}}32.6^{\text{s}}$, $\delta = 72^{\circ}50'55''$, $7''$ east of the distant giant elliptical galaxy (see Figure 6). This arc is quite bright (at $I = 20.90$, $V = 21.39$), and it is worth noting that the

comparatively bright arc magnitude places WL 1312.5+7252 among the very small number of clusters at $z > 0.5$ that are known to produce strongly lensed arcs that are sufficiently bright for spectroscopic studies. The only other such examples known to us are CL2236-04 (Melnick et al. 1993) and RCS 0224-0002 (Gladders, Yee, & Ellingson 2002).

If this arc is indeed a strongly lensed galaxy, the separation between the arc and the giant elliptical galaxy can be used to make a rough estimate of the mass of WL 1312.5+7252.

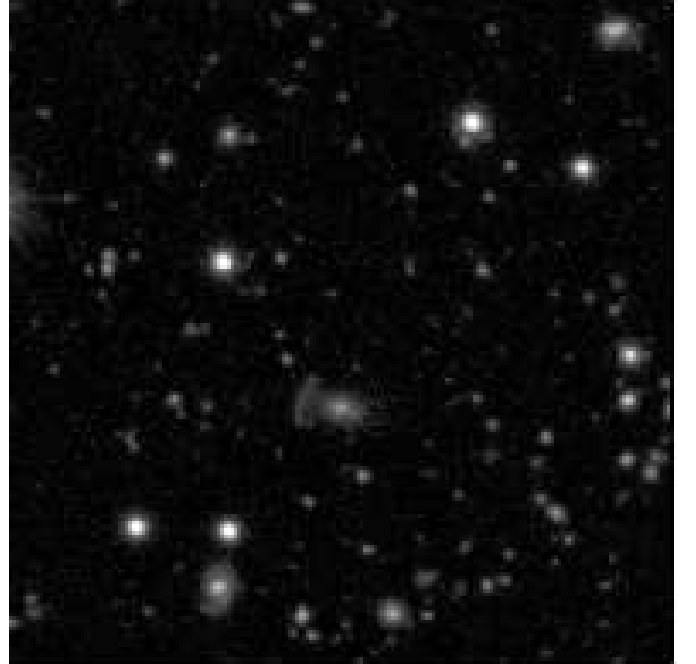


FIG. 6.— A blue arc curving around the central galaxy of the $z = 0.55$ cluster candidate WL 1312.5+7252 in the field of Abell 1705. North is up; east to the left and the FOV is $2' \times 2'$. This area is marked by the dotted lines in Fig. 5.

Assuming a SIS-type mass distribution centered on a giant elliptical galaxy at redshift $z_l = 0.6$, and assuming that the lensed arc is situated at the Einstein radius θ_E , we estimate a velocity dispersion $\sigma_{\text{arc}} = c\sqrt{(\theta_E w_s)/(4\pi w_{ls})} \simeq 900 \text{ km s}^{-1}$ for $z_s = 1$ and $\sigma_{\text{arc}} \simeq 700 \text{ km s}^{-1}$ for $z_s = 2$. The numbers above are calculated for the case of an Einstein-de Sitter Universe, where $w = 1 - (1+z)^{-1/2}$. The estimated velocity dispersion of 1150 km s^{-1} for WL 1312.5+7252 (see Table 1) comes from a SIS-model fit to the tangential weak shear averaged in radial bins centered on the mass peak. This high value and the high aperture mass value M_{ap} provides evidence for a relatively low arc redshift. The mass-to-light ratio listed in Table 1 is measured within R_{ap} and is based on galaxies in the color range $2.0 < V-I < 2.8$. The lower limit of this color interval was chosen to avoid foreground galaxies associated with A1705, and the upper limit was chosen to avoid background galaxies that are significantly redder than the red sequence of WL 1312.5+7252. The M/L_B value is consistent with a normal luminous cluster, and assuming a redshift-dependence $L_B \propto (z+1)$ for the luminosity evolution, the present-day value would be $M/L_B = (268 \pm 84)h$.

The only pointed X-ray observation of WL 1312.5+7252 is a 3.8 ksec EINSTEIN IPC exposure. In the IPC image there is diffuse emission from the main A1705 cluster extending in the direction of WL 1312.5+7252. Also, there is a hint of diffuse emission extending towards the mass structure southeast of the

main cluster. The bright X-ray point source, RX J1313.5+7259, located northeast of the main cluster masks any signs of diffuse emission that might be associated with the feature in the mass map in this direction.

KS93 $\kappa(r)$ RECONSTRUCTION

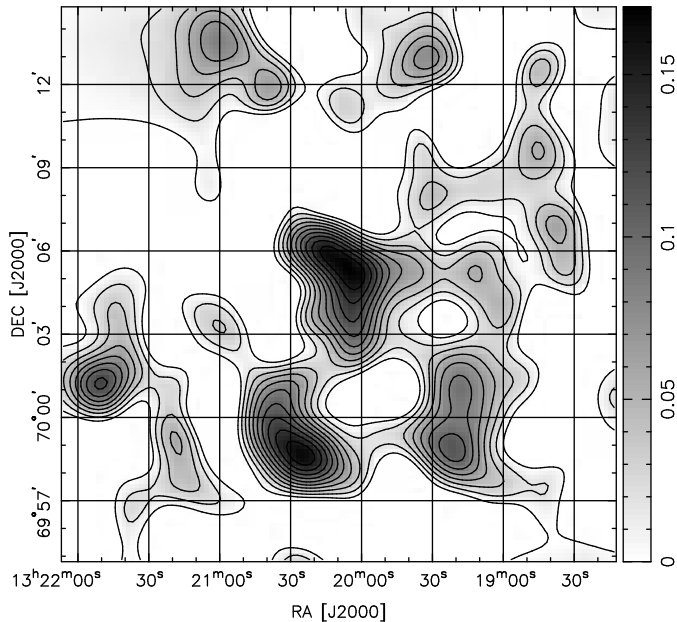


FIG. 7.— The reconstructed projected mass density in the field of A1722. The mass map is based on the KS93 inversion method, with a Gaussian smoothing scale of $47''$. The scale bar on the right runs from zero to the peak value of κ . The plotted contours start at zero and are spaced at intervals of $\Delta\kappa = 0.017$.

If WL 1312.5+7252 is at a redshift of $z = 0.55$, within a radius of r_{500} it is at least a factor three X-ray under-luminous relative to the expectation from the mass-X-ray luminosity relation of Reiprich and Böhringer (2002). Again, given the scatter in the mass-luminosity relation of an order of magnitude, WL 1312.5+7252 could be a rather normal cluster by X-ray standards.

In conclusion, information from galaxy photometry, (probable) strong lensing and weak lensing all indicate the presence of a new massive, high-redshift cluster in the field of A1705. Although the cluster is not detected in existing X-ray data, the X-ray constraints on the cluster are consistent with the expected cluster X-ray luminosity, but places the cluster at the faint end of the observed distribution of X-ray luminosities for the given mass. It would of course be of great interest to accurately measure the redshift of this cluster, and of the arc, to obtain definite confirmation of the lensed nature of the arc and to increase the accuracy of mass estimates of WL 1312.5+7252 from strong and weak lensing. Furthermore, Chandra or XMM-Newton observations are crucial to determine the hot gas content of the cluster and to independently map the mass distribution.

3.3. The A1722 Field

The cluster center of A1722 is dominated by a single cD galaxy. A $17''$ long, thin blue gravitationally lensed arc is visible $18''$ southwest of the cD. As shown in the mass map (Figure 7), there is a second peak in the mass distribution, WL 1320.4+6959, which is almost as significant as the mass peak corresponding to A1722 (its peak value is $\kappa = 0.166$). Figure 8 shows the distribution of red ($V-I > 2.2$) galaxies in the field. A concentration of galaxies is seen close to the position of WL

1320.4+6959, but with a larger spread in galaxy colors than the WL 1312.5+7252 cluster in the field of A1705. There appears to be a general overdensity of red galaxies in the southern part of the A1722 field, and there are several galaxy concentrations along a filamentary structure running along the southern part of the field. The same general appearance is evident in the panels corresponding to $V-I > 2.0$ in Figure 9.

The apparent early-type galaxy sequence associated with the galaxy concentration around WL 1320.4+6959 is less well-defined than for WL 1312.5+7252, but there appears to be a concentration of galaxies with colors around $V-I = 2.25$, corresponding to an estimated redshift of $z = 0.45 \pm 0.05$. A corresponding strong density peak is seen for galaxies in the range $1.9 < V-I < 2.5$ in Figure 9. As shown in Figure 10, there is an offset of $\sim 1'$ between this galaxy density peak and the

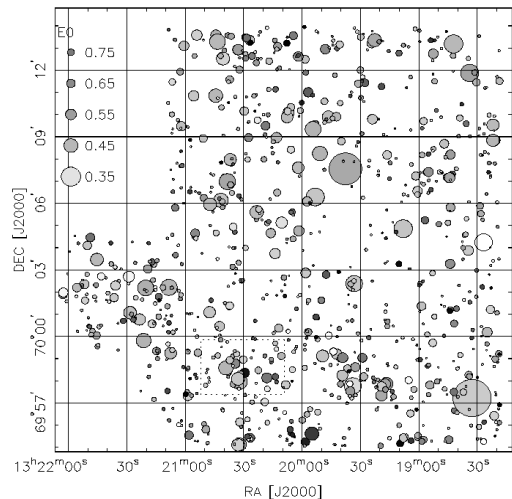


FIG. 8.— The reddest galaxies ($V-I > 2.2$) in the field of Abell 1722. The area of the circles is proportional to the I -band flux. The legend in the upper left corner indicates the flux and color (assuming no evolution of the SED) of an L_* E0 galaxy at a given redshift. The rectangular region denoted by the dotted lines indicates the region shown in Fig. 9. The lack of data in the lower left (southeastern) corner of the image is caused by obscuration by the guide probe when obtaining the I -band data for this field.

WL 1312.5+7252 mass peak. A red galaxy with an extended envelope is located within the innermost contour of the galaxy density peak, and appears to be the central galaxy of the cluster. The two last panels of Figure 9 show a moderate number density peak of very red ($2.65 < V-I < 3.1$) galaxies located even closer to the WL 1320.4+6959 mass peak. A color of $V-I = 2.9$ places the galaxies in this peak at $z \sim 1$ or higher, but any cluster at this redshift would have to be unrealistically massive to produce the observed weak lensing signal, since most of the source galaxies used in the lensing analysis are situated at lower redshifts. We therefore believe that the clustering of galaxies at $z \sim 0.45$ is chiefly responsible for producing the peak in pro-

jected mass density distribution. The first five panels in Figure 9 ($1.15 < V-I < 2.05$) also show moderate galaxy density peaks close to WL 1320.4+6959. Thus, it is possible that a projection of multiple structures along the line of sight, some of them possibly associated with A1722, are contributing to the WL 1320.4+6959 mass peak. Alternatively, we may just be seeing galaxies of different colors and morphological types at a single redshift. In this case, the significant scatter seen in the red cluster sequence suggests that the cluster is less dense and has a larger fraction of late-type galaxies than WL 1312.5+7252, which would be expected for a cluster which is still forming. Spectroscopic determinations of galaxy redshifts in the area of WL 1320.4+6959 would be required to conclusively distinguish between these two scenarios.

From an ASCA SIS 66 ksec exposure, the upper limit on the X-ray luminosity from WL 1320.4+6959 is a factor two below the expectation from the mass-luminosity relation of Reiprich & Böhringer (2002). However, the upper limit on the X-ray luminosity is uncertain by a factor two due to the uncertain subtraction of X-ray emission from the main cluster and a bright point source (seen in an archival 27 ksec ROSAT HRI exposure) southwest of the main cluster. Although WL 1320.4+6959 is X-ray underluminous, existing X-ray data are consistent with a cluster at redshift of $z \sim 0.45$.

The mass-to-light ratio listed in Table 1 is measured within R_{ap} and is based on galaxies in the color range $2.0 < V-I < 2.6$. The lower limit of this color interval was chosen to avoid foreground galaxies associated with A1722 (see Figure 9), and the upper limit was chosen to avoid background galaxies that are significantly redder than the apparent red sequence associated with WL 1320.4+6959. The M/L_B value is consistent with a normal luminous cluster, and assuming $L_B \propto (z+1)$ luminosity evolution, the present-day value would be $M/L_B = (429 \pm 171)h$.

4. DISCUSSION

Using weak gravitational lensing data, we have in the previous paragraphs identified three prominent (projected) mass concentrations representing new galaxy cluster (or sub-cluster) candidates. We use two-color, V - and I -band photometry to investigate the nature of these structures and make rough redshift estimates.

The first mass concentration, WL 1017.3+5931, is the most enigmatic of these objects. The morphology of the mass peak and the associated X-ray emission suggest a possible association with the nearby $z = 0.29$ cluster A959, but we find no overdensity of early-type cluster galaxies at the location of WL 1017.3+5931. There is also no strong evidence for clustering of galaxies at any other redshift at this position. This object remains a good candidate for an optically “dark” (sub-)cluster. The upper limit on the X-ray luminosity leaves the possibility that it is an X-ray (underluminous) cluster at or beyond the redshift of A959. Deep X-ray data of this system would be particularly interesting in order to accurately measure its hot gas content.

The second mass concentration, WL 1312.5+7252, appears to be associated with a rich cluster at $z \sim 0.55$ which also acts as a strong lens. This structure is associated with a prominent overdensity of red galaxies and has a prominent red galaxy sequence. Thus, it is likely to constitute a single strong physical overdensity of dark matter and galaxies, rather than being caused by a line-of-sight projection of lesser structures. Its M/L_B value is similar to the typical values of clusters selected

from baryonic tracers. The conservative upper limit on the X-ray luminosity of WL 1312.5+7252 is consistent with a cluster at $z \sim 0.55$ with the mass determined from weak lensing. However, WL 1312.5+7252 could well be an X-ray dark mass concentration, containing only a small amount of hot gas.

The third mass concentration, WL 1320.4+6959, is associated with an overdensity of galaxies at an estimated redshift of $z \sim 0.45$, but these galaxies show a larger spread in $V-I$ color than the galaxies in the WL 1312.5+7252 cluster. However, the upper limit on its X-ray emission does not allow us to rule out that WL 1320.4+6959 is a single cluster at $z \sim 0.45$ which is X-ray underluminous and possibly X-ray dark. It is thus unclear whether this density peak represents a chance superposition of objects at different redshifts or whether it represents a single cluster at $z \sim 0.45$ which is still forming and is not yet virialized. Weinberg & Kamionkowski (2002) estimate the abundances of non-virialized, X-ray underluminous protoclusters that will be detectable in weak lensing surveys, and they find that such systems are likely to be detected in surveys comparable to ours. The M/L_B value we find is typical for a normal optically luminous cluster.

At this point we may speculate whether it is significant that we find three mass concentrations with $\kappa > 0.15$ based on 1.0 deg^2 of imaging of fields containing massive clusters, while Wilson et al. (2001) find no such objects from similar data (1.5 deg^2 of imaging) of blank fields. We also recall that the two optically dark mass concentrations previously discovered by Erben et al. (2000) and Umetsu & Futamase (2000) were both found in the fields of massive clusters. In the case of WL 1312.5+7252 we are seeing a mass concentration which is clearly physically unrelated to the nearby Abell cluster. For WL 1320.4+6959 it is hard to draw an equally firm conclusion, since, as noted in § 3.3, there may be a significant contribution to the projected mass density from structures at the redshift of A1722.

The photometric data for WL 1017.3+5931 do not provide any strong evidence for an association with nearby A959, but the morphology of the mass peak does suggest a possible physical link between the two objects. In a recent study, White, van Waerbeke & Mackey (2002) show that significant peaks in the projected density distribution, resembling clusters with virial masses of $10^{14} - 3 \times 10^{14} h^{-1} M_{\odot}$ may be generated by line-of-sight projections of multiple correlated structures with $M < 10^{14} h^{-1} M_{\odot}$. It is possible that WL 1017.3+5931 is such an object, generated by a superposition of $\sim 10^{13} h^{-1} M_{\odot}$ halos within the overdensity associated with A959. This scenario would naturally explain the low X-ray luminosity, but does not predict an unusually high M/L_B value or the lack of an associated peak in the galaxy density distribution.

Clearer answers to the nature of weak lensing-detected mass concentrations may come soon from systematic cluster searches in the deep wide-field imaging data sets currently used for measurements of “cosmic shear”. The sky area collectively probed by such surveys to similar depth is now at least an order of magnitude larger than the sky area we study here (see e.g., van Waerbeke et al. 2001).

Our results also demonstrate the usefulness of multi-color photometry and color slicing techniques when interpreting results from weak lensing cluster searches. At redshifts $z \sim 0.5$ and higher, even rich clusters do not represent strong galaxy density enhancements in single-passband imaging data. In the case of WL 1320.4+6959, an optical counterpart to the mass

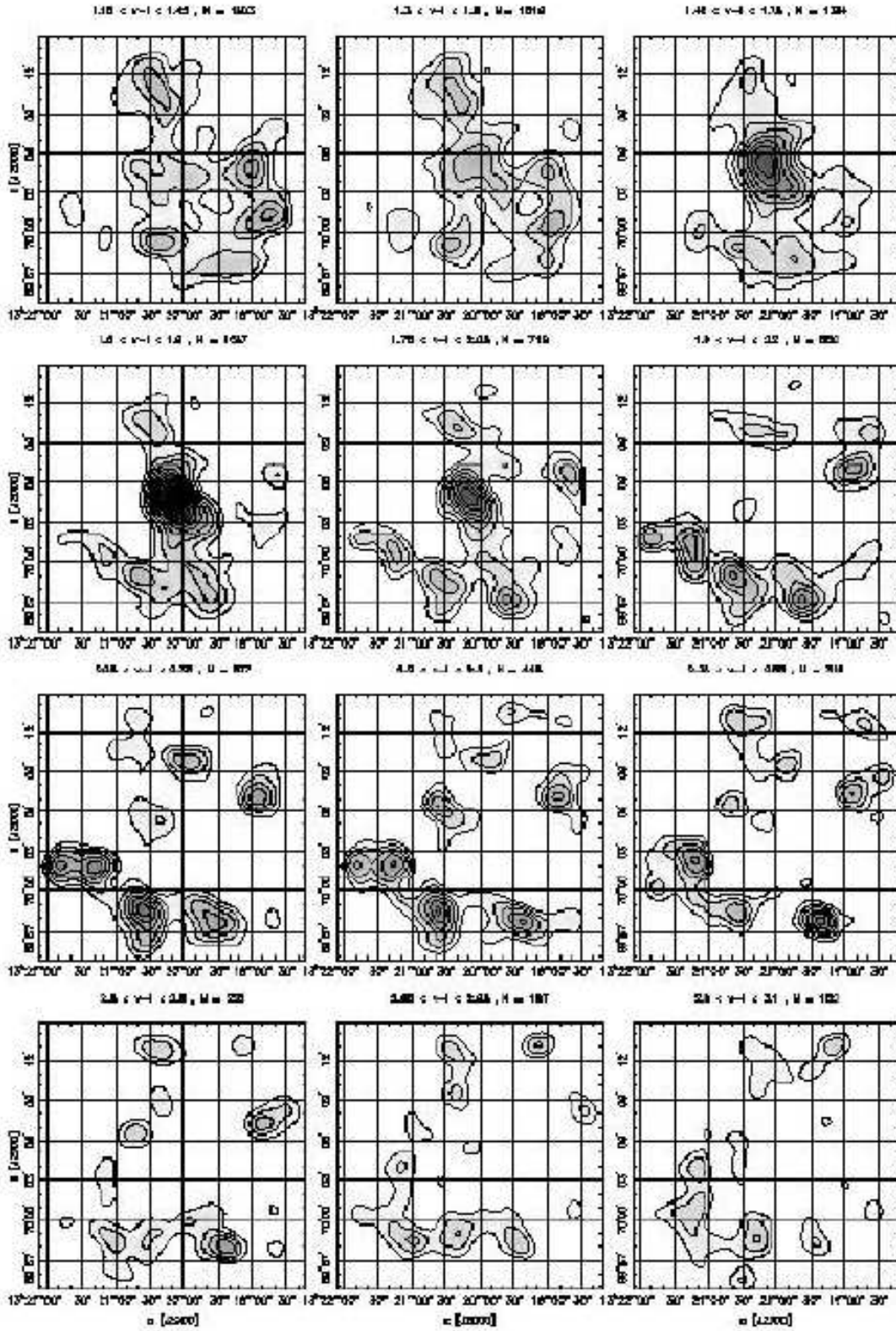


FIG. 9.— The surface number density distribution of $I < 23.0$ galaxies in various $V-I$ color intervals in the field of A1722. See the caption of Fig. 2 for details.

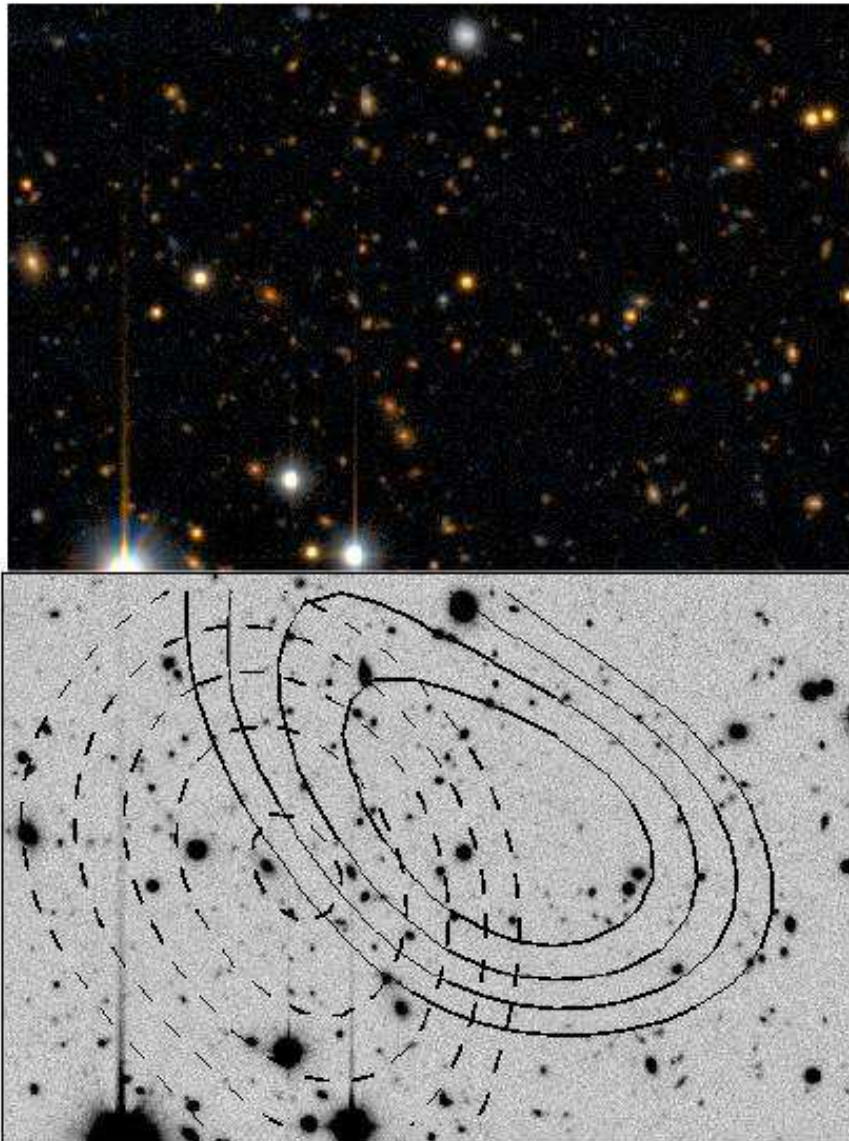


FIG. 10.— The plots show a $225'' \times 150''$ region around the WL 1320.4+6959 mass peak in the field of A1722. Top: “True color” image based on 4.5h of integration in the V -band and 4h of integration in the I -band. Bottom: Solid lines show contours of the projected mass density κ indicating the WL 1320.4+6959 mass peak. Contour levels start at $\kappa = 0.1$ and are plotted at intervals of 0.02 in κ . The dashed lines are contours of the smoothed galaxy density distribution in the $2.2 < V-I < 2.5$ subpanel in Figure 9.

concentration could not be identified before data in a second passband had been obtained. It is also clear that X-ray data from either Chandra or XMM-Newton are required in order to detect or tightly constrain the hot gas content of the detected (sub-)clusters.

The methodology for cluster searches may be further refined in the future by developing a more objective and quantitative search algorithm that combines weak gravitational lensing information with e.g. the cluster-red-sequence method of Gladders & Yee and/or X-ray data. The X-ray data would be particularly useful for separating line-of-sight superpositions of less massive objects (which would be a significant source of noise and bias for both optical and weak lensing data; see e.g., Hoekstra 2001; White et al. 2002) from genuine deep potential wells. This would greatly improve the power of such surveys to constrain cosmological models.

We thank the anonymous referee for suggestions that have

improved our work and its presentation. We also thank Harald Ebeling, Jens Hjorth, Henk Hoekstra, Gerry Luppino, Somak Raychaudhury, and Gillian Wilson for useful comments and discussions. We thank the staff of the University of Hawaii 2.24m telescope and the Nordic Optical Telescope for support during our observing runs. HD gratefully acknowledges support from a doctoral research fellowship awarded by the Research Council of Norway. HD and PBL thank the Research Council of Norway for travel support. KP acknowledges support from the Danish National Research Council. This research has made use of the NASA/IPAC Extragalactic Database (NED) which is operated by the Jet Propulsion Laboratory, California Institute of Technology, under contract with the National Aeronautics and Space Administration. This research has made use of data obtained from the High Energy Astrophysics Science Archive Research Center (HEASARC), provided by NASA's Goddard Space Flight Center.

REFERENCES

- Abazajian, K., Fuller, G. M., & Tucker, W. H. 2001, *ApJ*, 562, 593.
 Abell, G. O. 1958, *ApJS*, 3, 211
 Bertin, E., & Arnouts, S. 1996, *A&AS*, 117, 393
 Briel, U., & Henry, J. P. 1993, *A&A*, 278, 379
 Böhringer, H. et al. 2000, *ApJS*, 129, 435
 Carlberg, R. G., Yee, H. K. C., & Ellingson, E. 1997, *ApJ*, 478, 462
 Dahle, H., Kaiser, N., Irgens, R. J., Lilje, P. B., & Maddox, S. J. 2002, *ApJS*, 139, 313 (Paper I)
 Dickey, J.M. & Lockman, F.J., 1990, *Ann.R.A&A.*, 28, 215
 Erben, T., van Waerbeke, L., Mellier, Y., Schneider, P., Cuillandre, J.-C., Castander, F. J., & Dantel-Fort, M. 2000, *A&A*, 355, 23
 Ettori, S. & Fabian, A. C. 1999, *MNRAS*, 305, 834
 Fahlman, G., Kaiser, N., Squires, G., & Woods, D. 1994, *ApJ*, 437, 56
 Finoguenov, A.; Reiprich, T. H.; Böhringer, H. 2001, *A&A*, 368, 749
 Fischer, P. 1999, *AJ*, 117, 2024
 Gladders, M. D. & Yee, H. K. C. 2000, *AJ*, 120, 2148
 Gray, M. E., Ellis, R. S., Lewis, J. R., McMahon, R. G., & Firth, A. E. 2001, *MNRAS*, 325, 111
 Hansen, S. H., Lesgourgues, J., Pastor, S., & Silk, J. 2002, *MNRAS*, 333, 544
 Hoekstra, H. 2001, *A&A*, 370, 743
 Hoekstra, H., Franx, M., Kuijken, K., & van Dokkum, P. G. 2002, *MNRAS*, 333, 911
 Irgens, R. J., Lilje, P. B., Dahle, H., & Maddox, S. J. 2002, *ApJ*, 579, 227 (Paper II)
 Kaiser, N. 2000, *ApJ*, 537, 555
 Kaiser, N. & Squires, G. 1993, *ApJ*, 404, 441, KS93
 Kaiser, N., Squires, G., Fahlman, G., & Woods, D. 1994, in "Clusters of Galaxies", XXIXth Rencontres de Moriond, ed. F. Durret, A. Mazure, and J. Tran Thanh Van (Gif-sur-Yvette: Edition Frontières)
 Kaiser, N., Wilson, G., Luppino, G., & Dahle, H. 1999, preprint (astro-ph/9907229)
 Lubin, L. M. 1996, *AJ*, 112, 23
 Miralles, J.-M. et al. 2002, *A&A*, 388, 68
 Mushotzky, R. F. & Scharf, C. A. 1997, *ApJ*, 482, L13
 Reiprich, T. H. & Böhringer, H. 2002, *ApJ*, 567, 716
 Smail, I., Edge, A. C., Ellis, R. S., & Blandford, R. D. 1998, *MNRAS*, 293, 124
 Stanford, S. A., Eisenhardt, P. R., & Dickinson, M. 1998, *ApJ*, 492, 461
 Umetsu, K. & Futamase, T. 2000, *ApJ*, 539, L5
 Van Waerbeke, L. et al. 2001, *A&A*, 374, 757.
 Weinberg, N. N. & Kamionkowski, M. 2002, *MNRAS*, 337, 1269
 White, M., van Waerbeke, L., & Mackey, J. 2002, *ApJ*, 575, 640
 Wilson, G., Kaiser, N., & Luppino, G. A. 2001, *ApJ*, 556, 601
 Wittman, D., Tyson, J. A., Margoniner, V. E., Cohen, J. G., & Dell'Antonio, I. P. 2001, *ApJ*, 557, L89